Materials Science & Engineering A 573 (2013) 166–174

Contents lists available at SciVerse ScienceDirect

Materials Science & Engineering A

journal homepage: www.elsevier.com/locate/msea

Impurity scavenging, microstructural refinement and mechanical properties of powder metallurgy titanium and titanium alloys by a small addition of cerium silicide

Y.F. Yang, S.D. Luo, G.B. Schaffer, M. Qian *

The University of Queensland, School of Mechanical and Mining Engineering, ARC Centre of Excellence for Design in Light Metals, Brisbane, Qld 4072, Australia

ARTICLE INFO

Article history:
Received 17 November 2012
Received in revised form
14 February 2013
Accepted 15 February 2013
Available online 14 March 2013

Keywords:
Titanium alloys
Powder metallurgy
Sintering
Grain refinement
Rare earth

ABSTRACT

A small addition (≤0.5 wt%) of cerium silicide ($CeSi_2$) to powder metallurgy (PM) commercially pure Ti (CP-Ti), Ti–6Al–4V and Ti–10V–2Fe–3Al (all in wt%) results in substantial microstructural refinement and noticeably improved ductility with marginally improved sintered density. $CeSi_2$ is unstable and decomposes between 1423 K and 1473 K. The Si goes into solid solution in β-Ti and is responsible for the improved sintered density while the Ce scavenges both oxygen (O) and chlorine (Cl) from the Ti powder and therefore improves tensile ductility. The resulting CeO_2 and $CeCl_xO_y$ particles generally exist along or close to the prior-β grain boundaries. The substantial microstructural refinement in terms of both the prior-β grain size and the subsequent α-Ti lath size is attributed to the grain boundary pinning effect of the CeO_2 particles. The optimum concentration of $CeSi_2$ is approximately 0.5 wt%, beyond which both the sintered density and tensile elongation drop with increasing addition of $CeSi_2$. $CeSi_2$ can be a practical form of Ce addition to PM Ti alloys for impurity scavenging, microstructural refinement and tensile ductility improvement.

1. Introduction

Powder metallurgy (PM) offers the potential for cost-effective fabrication of titanium (Ti) components for a wide range of applications [1–3]. Oxygen (O) is an important issue that affects this potential in terms of both the cost of production and the resulting mechanical properties. Recent studies have revealed that the tensile elongation of PM Ti–6Al–4V (all compositions are given in wt% herein) changed little with increasing oxygen content from 0.2 wt% to ~0.32 wt% [4,5] but dropped from >10% to <5% once the oxygen content exceeded ~0.32 wt%, and further to <2% when the oxygen content was >0.45 wt% [4]. The oxygen content of an as-sintered Ti alloy largely depends on the oxygen content of the Ti powder. Currently, most inexpensive hydride–dehydride (HDH) Ti powder products contain ≥0.25 wt% oxygen. The powder handling and sintering process can readily add an extra 1000 ppm of oxygen, exceeding the critical value of 0.32 wt%. Being able to effectively mitigate the detrimental effect of oxygen on ductility is thus important for the fabrication of low-cost high-performance Ti alloys using inexpensive HDH Ti powder.

The Ellingham diagram [6] indicates that at a typical sintering temperature of ≥1473 K for PM Ti, only rare earth (RE) elements are practical to scavenge oxygen from titanium. In the 1970s and 1980s, RE elements were widely introduced into Ti alloys by rapid solidification processing (RSP) [7–31] and the formation of RE oxides was investigated both theoretically and experimentally [27]. The RSP led to metastable supersaturation of RE and O in Ti. As a result, precipitation of fine RE oxides occurred during subsequent heat treatment through the scavenging of O by the RE elements. In the presence of excessive oxygen, the resulting RE oxides would evolve to the most stable stoichiometric particle [27]. The presence of these fine RE oxides enhanced the elevated-temperature strength by dispersion hardening of the final RSP product forms consolidated from powder, flake, ribbon, fiber, etc. However, the resulting tensile ductility was barely affected as the initial oxygen content in the Ti alloy ingot was already very low [14–18]; there was no need to scavenge the oxygen from a ductility perspective. In the 1990s, RE elements were introduced into PM Ti alloys in the form of RE-containing compounds (most notably as RE oxides) [32–34]. Because most RE oxides are not oxygen deficient, they fail to scavenge oxygen from the Ti powder. As a result, the resulting tensile elongation showed little improvement [32–34]. The benefits of using RE elements to improve the tensile ductility of as-sintered PM Ti alloys were first demonstrated by Liu and co-workers [35,36]. They introduced RE elements to PM Ti alloys in the form of a 60Al–40Nd (at%) master alloy powder and achieved substantially improved tensile ductility. Subsequently, Zhang et al. [37] mixed mechanically crushed neodymium (Nd)

* Corresponding author. Tel.: +61 7 3365 4185; fax: +61 7 3346 7015.
E-mail address: ma.qian@uq.edu.au (M. Qian).

0921-5093/$ - see front matter © 2013 Elsevier B.V. All rights reserved.
http://dx.doi.org/10.1016/j.msea.2013.02.042

Table 1
Summary of rare earth (RE) additions to PM Ti alloys.

Addition form	Alloy (wt%)	Addition level (wt%)	Relatively sintered density (%)	UTS (MPa)	YS (MPa)	Elongation (%)
60Al–40Nd (at%) master alloy [22]	Ti–6Al–4V	0	~97	~1030	–	~2.5
		0.3	~97.5	~1050	–	~11
		0.8	~97.5	~990	–	~12
		1.2	~97.2	~940	–	~13
60Al–40Nd (at%) master alloy [22]	Ti–1Fe–1Mo–4.5Al	0	~97.2	~850	–	~1
		0.3	~97.9	~950	–	~2
		0.8	~97.7	~950	–	~3
		1.2	~97.7	~920	–	~5
LaH_2 [22,26]	Ti–1.5Fe–2.25Mo	0	~93	~685	~634	~4.8
		0.15	~94	~710	~650	~5
		0.3	~95	~740	~660	~8
		0.6	~95.9	~770	~690	~5.5
		1.2	~95.5	~760	~685	~5.4
		3.0	~95.2	~710	~640	~7
YH_2 [24,26]	Ti–1.5Fe–2.25Mo	0	–	~685	~634	~4.8
		0.6	–	~645	~553	~7.6
LaB_6 [22,26]	Ti–1.5Fe–2.25Mo	0	~93	~685	~634	~4.8
		0.15	~94	~759	~650	~7
		0.3	~93.8	~720	~645	~4
		0.6	~93.2	~700	~640	~3.8
		1.2	~91.8	~650	~580	~2.8
		3.0	~87	~640	~575	~2.5

UTS: ultimate tensile strength; YS: yield strength (0.2% offset).

metal powder (<100 μm) with Ti–6Al–4V alloy powder in argon and consolidated the powder mixtures by a laser rapid forming (LRF) process. The tensile elongation increased from ~4% to ~9% with an addition of 0.2 wt% Nd but dropped beyond that. Nevertheless, it is not very practical to introduce pure RE elements to PM Ti. Recently, Liu et al. [38–41] introduced RE elements to PM Ti alloys in various forms, including RE boride (LaB_6) powder or RE hydride (LaH_2, YH_2) powder etc., and achieved noticeably improved tensile ductility. Table 1 summarizes these efforts. Recent detailed studies of the addition of YH_2 powder to PM CP-Ti and Ti alloys revealed that YH_2 decomposed into pure yttrium (Y) and the scavenging of oxygen occurred through the formation of a range of oxygen-deficient Y_xO_y compounds with the same crystal structure as Y_2O_3 [42,43]. Also, the addition of YH_2 simultaneously scavenged chlorine (Cl) from the Ti powder leading to the formation of essentially oxygen-free binary Y–Cl compounds [42].

The use of Al–Nd master alloy powder is not suited to low Al content or Al-free PM Ti alloys. RE boride powder is a useful form of RE addition but the simultaneous introduction of B, even at a small amount (≤0.3 wt%), may offset the improvement in ductility. The use of RE hydride powder such as LaH_2 and YH_2 powder allows the introduction of pure RE elements to PM Ti alloys. However, they are not commercially available and are prone to oxidation when exposed to air. Hence, it would be useful to identify a different form of RE addition.

Cerium silicide ($CeSi_2$) appears to be one such promising candidate: (i) it is commercially available and also stable at room temperature; (ii) it is more affordable (USD $4.52/g) than other forms of RE compounds (USD $6.7/g for LaB_6, USD $7.02/g for $LaSi_2$) [44]; (iii) compared to B, Si has a good solubility in α-Ti. This permits a high level of RE addition for significant scavenging of oxygen without forming brittle silicides; and (iv) a small addition of Si (0.5 wt%) is effective in enhancing the densification and strengthening of PM Ti alloys [45,46]. To date, no information exists about the use of $CeSi_2$ in PM Ti alloys. It is unknown if $CeSi_2$ will be able to scavenge oxygen and chlorine from the Ti powder and how the mechanical properties will respond accordingly.

This paper investigates the effect of a small addition of $CeSi_2$ on the impurity scavenging, sintering densification, microstructure and mechanical properties of PM CP-Ti (Grade 2), Ti–6Al–4V and Ti–10V–2Fe–3Al. These three Ti materials are selected because of their commercial importance and their established microstructure–property relationships in the as-sintered state by the cold-compaction-and-sinter process.

2. Experimental procedure

HDH Ti powder (99.5% purity, 0.25%O, 0.05%Cl, −250 mesh), supplied by Kimet, China, and two master alloy powders, 66.7V–13.3Fe–20Al (in wt%, 99.5% purity, −325 mesh) and 58V–42Al (in wt%, 99.5% purity, −325 mesh), supplied by Baoji Jia Cheng Rare Metal Materials Co. Ltd., China, were used. Aluminum powder (99.7% purity, ~3 μm), supplied by Aluminum Powder Company Ltd., UK, was used to balance the composition of Ti–6Al–4V alloy due to the use of the 58V–42Al master alloy powder. A small ingot of $CeSi_2$ (99.5% purity) supplied by Alfa Aesar was crushed into powder by manual grinding for 2 min in a mortar at room temperature. To distinguish between the roles of Ce and Si introduced as $CeSi_2$ in sintering densification, the equivalent amount of elemental Si powders (≤45 μm, 99.5% purity, supplied by the CERAC Inc., USA) were introduced to the powder mixture of Ti–10V–2Fe–3Al alloy. The cold compaction process was similar to that described in a previous study [47]. Green tensile bars with dimensions of approximately 3.3 mm×3.5 mm cross-section and 18.6 mm gauge length (total length: 56.6 mm) were compacted at 600 MPa in a floating die specially designed for tensile testing. The as-sintered tensile samples measured about 3.25 mm×2.9 mm cross-section and 15 mm gauge length.

Sintering was conducted at 1623 K for 120 min in a tube furnace under a vacuum of 10^{-3}–10^{-2} Pa, with heating and cooling both at 4 K/min. The sintered density was measured by the Archimedes method following the ASTM standard B328. Samples cut from tensile bars were polished using 50 nm colloidal alumina. Polished samples of as-sintered Ti–6Al–4V and Ti–10V–2Fe–3Al were examined without etching but to reveal the grain boundaries, polished samples of as-sintered CP-Ti were etched with Kroll's etchant. The microstructure was analyzed using scanning electron microscopy (SEM, Model JEOL 6460L, Tokyo, Japan) equipped with energy-dispersive spectroscopy (EDS, Model JEOL, JEOL Ltd., Tokyo, Japan). Differential scanning calorimetry (DSC, Model Netzsch STA 409CD, Wittelsbachestraße, Germany) was used to determine the stability of $CeSi_2$ and the interaction between Ti and $CeSi_2$ in Ti–1.0$CeSi_2$ powder mixtures during heating to 1623 K. The Image-Pro plus 5.0 software (Media Cybernetics, Bethesda, MD, USA) was used to quantify the microstructure. For each as-sintered material, the average prior-β grain size was measured from 500 grains and the average length of the α-Ti laths in as-sintered Ti–6Al–4V and Ti–10V–2Fe–3Al was measured from 1000 α-Ti laths. X-ray diffraction (XRD, D8 Advance, Cu Kα target, Bruker AXS, Madison, WI, USA) was used for phase identification. Tensile testing was conducted on an Instron screw machine (Model 5054, Instron Corporation, 145 Norwood, MA, USA) with a cross head speed of 0.5 mm/min. A video extensometer was used to record the displacement.

3. Results

3.1. Effect on densification

Fig. 1 shows the densities of CP-Ti, Ti–6Al–4V and Ti–10V–2Fe–3Al after sintering at 1623 K for 120 min as a function of $CeSi_2$ addition up to 1.0 wt%. The sintered density increased marginally up to an addition of 0.5 wt% $CeSi_2$ but decreased substantially afterwards up to an addition of 1.0 wt% $CeSi_2$. This was observed with all three PM Ti materials.

Fig. 2 shows the effect of the addition of elemental Si powder on the density of Ti–10V–2Fe–3Al after sintering at 1623 K for 120 min. Si consistently improves the sintered density of Ti–10V–2Fe–3Al. The equivalent Si content introduced as $CeSi_2$ is also plotted in Fig. 1. It is clear from Figs. 1 and 2 that the improvement in the sintered density with an addition of ≤0.5 wt% $CeSi_2$ originates from the Si contained in $CeSi_2$. No beneficial effect of Ce on the sintering densification can be inferred from the experimental results.

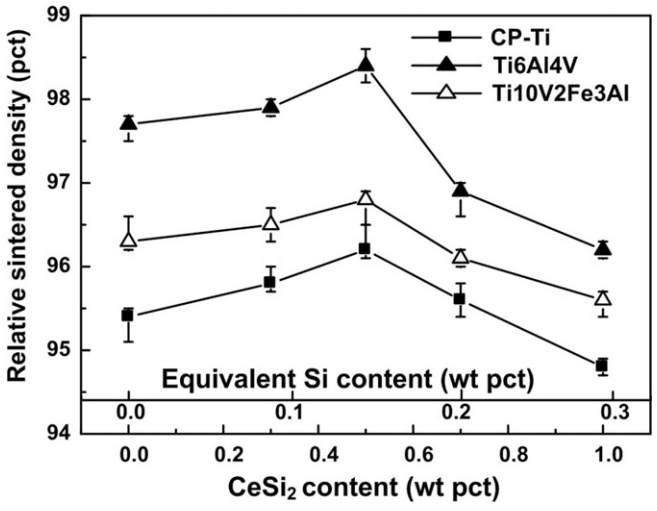

Fig. 1. Sintered density of CP-Ti, Ti–6Al–4V and Ti–10V–2Fe–3Al as a function of the addition of $CeSi_2$. Sintering was conducted at 1623 K for 120 min.

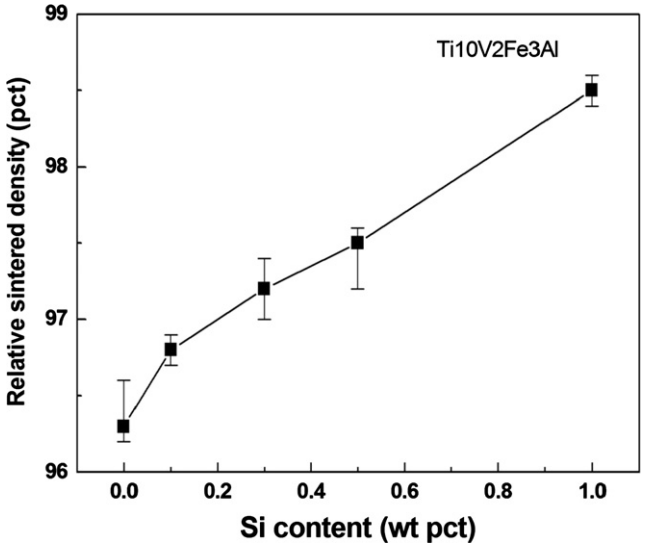

Fig. 2. Sintered density of Ti–10V–2Fe–3Al versus the addition of Si after sintering at 1623 K for 120 min.

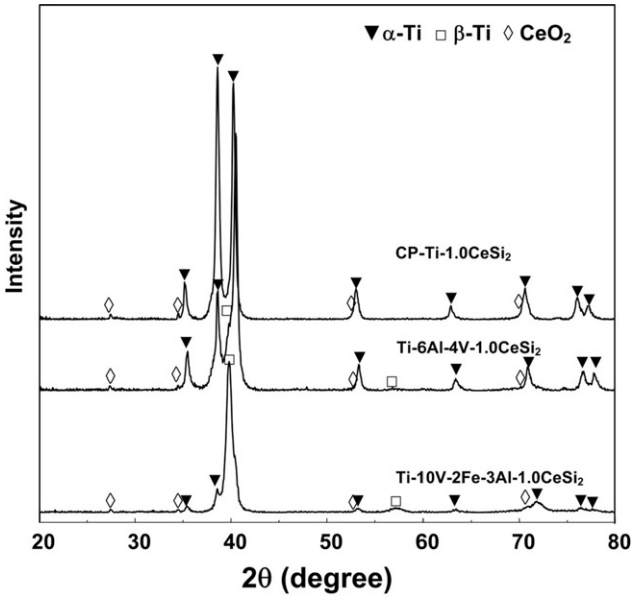

Fig. 3. XRD patterns of CP-Ti, Ti–6Al–4V and Ti–10V–2Fe–3Al with an addition of 1.0 wt% $CeSi_2$ after sintering at 1623 K for 120 min.

3.2. XRD and DSC results

Fig. 3 shows the XRD results of CP-Ti–1.0$CeSi_2$, Ti–6Al–4V–1.0$CeSi_2$ and Ti–10V–2Fe–3Al–1.0$CeSi_2$ sintered at 1623 K for 120 min. $CeSi_2$ disappeared in each case while CeO_2 formed. No titanium silicides were detected.

Fig. 4 shows the DSC results obtained from heating $CeSi_2$ powder and a Ti–1.0$CeSi_2$ powder mixture to 1623 K in argon at 10 K/min. The following observations are notable.

- $CeSi_2$: two significant endothermic peaks were observed at 1393 K and 1473 K, well below the melting point of $CeSi_2$ (1893 K), indicating that $CeSi_2$ was unstable and decomposed around these two temperatures.

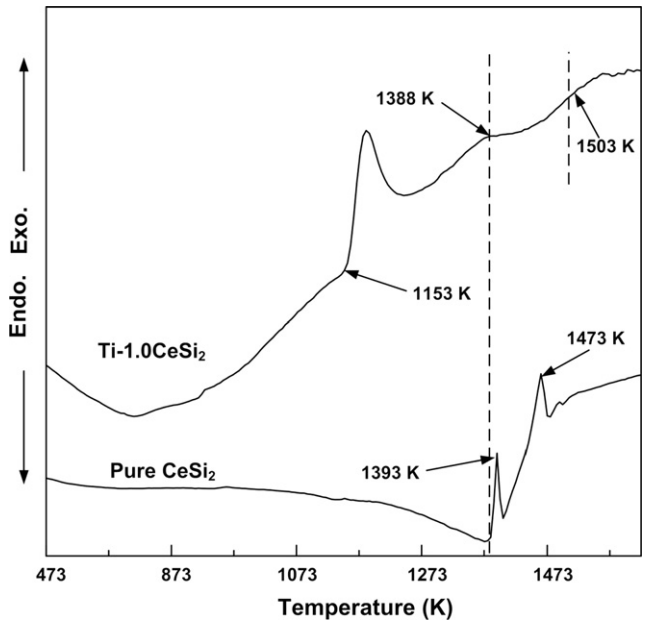

Fig. 4. DSC curves of $CeSi_2$ and Ti–1.0$CeSi_2$, heated at 10 K/min to 1623 K in argon.

- Ti–1.0$CeSi_2$: a substantial endothermic peak started to develop from ~1153 K, followed by a weak exothermic profile ranging from 1388 K to 1503 K. The endothermic peak corresponded to the α-Ti→β-Ti transformation. The formation of the weak exothermic profile will be discussed subsequently.

3.3. Microstructural evolution and refinement by $CeSi_2$

Fig. 5 shows the as-sintered microstructures of CP-Ti and CP-Ti–0.5$CeSi_2$. A large number of bright particles were observed in the as-sintered CP-Ti–0.5$CeSi_2$ (see Fig. 5b and c). They were confirmed by EDS to be all Ce-containing particles. Similar to yttrium-containing PM Ti alloys [42], spot EDS results revealed two different types of Ce-containing particles. One type is binary cerium oxides free of Cl (see Fig. 5d) and the other type of compounds contain predominantly Ce and Cl with only a small amount of oxygen (see Fig. 5e). This ternary $CeCl_xO_y$ phase was similarly observed in as-sintered Ti–6Al–4V–0.5$CeSi_2$ without etching (see Fig. 6c), confirming that the high Cl content detected was not from the etchant. No Si was detected in either type of particles. These results indicate that both O and Cl can be scavenged by Ce from the Ti matrix during sintering.

A closer inspection of the as-sintered microstructures of CP-Ti and CP-Ti–0.5$CeSi_2$ (see Fig. 5a and b) revealed that apart from the scavenging of O and Cl, there was significant microstructural refinement arising from the addition of $CeSi_2$. This was observed with Ti–6Al–4V and Ti–10V–2Fe–3Al too. Fig. 6 shows the as-sintered microstructures of Ti–6Al–4V and Ti–10V–2Fe–3Al with and without $CeSi_2$. Fig. 7 shows the detailed quantitative analyses of the prior-β Ti grain size in CP-Ti, Ti–6Al–4V and Ti–10V–2Fe–3Al and the average length of the α-Ti laths in Ti–6Al–4V and Ti–10V–2Fe–3Al as a function of the addition of $CeSi_2$. A remarkable refinement occurred at an addition of 0.3 wt% $CeSi_2$. After that, the grain size continued to decrease but at a much lesser degree. Similar observations were made of the refinement of the α-Ti laths. However, the width of α-Ti laths slightly increased (see Fig. 6). Also noticed is that the Ce-containing particles increased in size with increasing addition of $CeSi_2$.

3.4. Mechanical properties

Fig. 8 shows the tensile properties of CP-Ti, Ti–6Al–4V and Ti–10V–2Fe–3Al containing up to 1.0 wt% $CeSi_2$. Both the tensile strength and yield strength increase marginally with increasing addition of $CeSi_2$. The tensile elongation shows a noticeable increase with increasing addition of $CeSi_2$ up to 0.5 wt% but drops afterwards. For example, with an addition of 1.0 wt% $CeSi_2$, which introduces 0.71 wt% Ce and 0.29 wt% Si, the tensile elongation is even lower than without the addition in each case. Fig. 9 shows the fractographs of CP-Ti and Ti–6Al–4V alloys with additions of 0.5 wt% $CeSi_2$ and 0.7 wt% $CeSi_2$. The presence of CeO_2 particles is readily visible on the tensile fractographs, indicating that they have played a noticeable role in leading to the tensile fracture observed.

4. Discussion

4.1. The effect of $CeSi_2$ on sintering densification

Previous studies have indicated that RE additions do not normally enhance the sintering of PM Ti alloys, with the exception of LaH_2 in Ti–1.5Fe–2.25Mo (see Table 1). As noted earlier from Figs. 1 and 2, the increase in the sintered density from the addition of ≤0.5 wt% $CeSi_2$ arises from the Si rather than the Ce. Thermo-Calc calculations predicted that the solidus temperatures of Ti, Ti–6Al–4V and Ti–10V–2Fe–3Al decreased with increasing Si content. For instance, the predicted solidus temperatures are 1922 K for Ti–0.5Si (wt%) versus 1943 K for Ti, 1953 K for Ti–6Al–4V–0.5Si (wt%) versus 1971 K for Ti–6Al–4V, and 1851 K for Ti–10V–2Fe–3Al–0.5Si (wt%) versus 1880 K for Ti–10V–2Fe–3Al. A decrease in the solidus temperature favors sintering densification. The decline in the sintered density with an addition of >0.5 wt% $CeSi_2$ is consistent with previous observations that an excessive addition of RE elements resulted in lower sintered densities (see Table 1). The sintering of CP-Ti, Ti–6Al–4V and Ti–10V–2Fe–3Al with the addition of $CeSi_2$ still belongs to solid state sintering. The significant refinement of the prior-β grains (see Fig. 7a) and the microstructure characterization (see Fig. 6) revealed that the CeO_2 and $CeCl_xO_y$ particles are effective β-Ti grain growth inhibitors. In other words, they impeded the motion of the particle–particle interfaces during sintering and therefore hindered the sintering shrinkage. Also, it should be pointed out that the actual decline in the sintered density caused by Ce would have been much greater without the beneficial effect of Si.

The solubility of Ce in oxygen-free β-Ti at 1623 K is about 0.5 wt% [7]. With about 0.3 wt% O in solid solution in β-Ti at the sintering temperature, Ce is expected to first react with O before any solid solution develops because of the high chemical affinity of Ce for O. To reduce the O content in β-Ti from 0.3 wt% to 0.1 wt% requires an addition of 0.87 wt% Ce or equivalent to 1.0 wt% $CeSi_2$. This was the reason for limiting the addition of $CeSi_2$ to 1.0 wt%. Little solid solution of Ce in β-Ti at the sintering temperature was thus expected. This is supported by selected EDS spot analyses. In addition, no Ti–Ce intermetallics exist according to the Ce–Ti phase diagram. Hence the Ce introduced as $CeSi_2$ mainly exists as Ce-containing oxides and oxychlorides. Fig. 5 shows that these Ce-containing particles generally form along or close to the grain boundary. The formation of such excessive particles along the grain boundary area are expected to impede shrinkage, corresponding to the reduced sintered densities with an addition of >0.5 wt% $CeSi_2$.

4.2. The stability of $CeSi_2$ in PM Ti

$CeSi_2$ is a non-stoichiometric phase in which the Si content can vary from 64 at% to 66.67 at% ($CeSi_x$, $x=1.78$–2.0) [48–50].

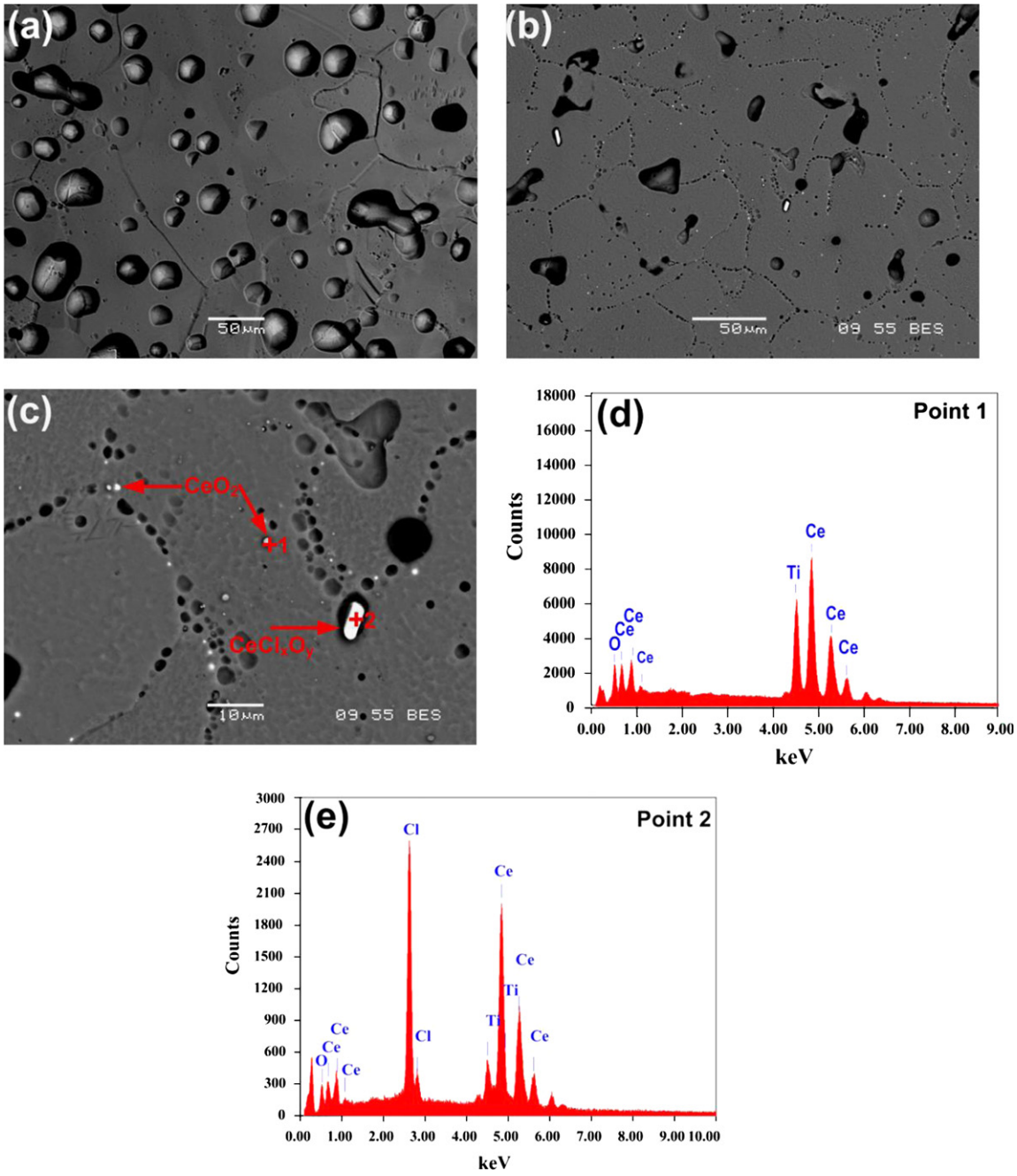

Fig. 5. As-sintered microstructures of (a) CP-Ti and (b) CP-Ti–0.5$CeSi_2$ (sintered at 1623 K for 120 min); (c) is a magnified view of (b); (d) is spot EDS of a CeO_2 particle (point 1) in (c); and (e) is spot EDS of a $CeCl_xO_y$ particle (point 2) in (c).

Hence $CeSi_2$ can decompose into $CeSi_x$+Si (x is from 1.78–2.0). The decomposition of $CeSi_2$ is endothermic while the formation of CeO_2 (oxidation) and $CeCl_xO_y$ (chlorination) is exothermic. These thermal events overlap each other, leading to a weak exothermic development stage on the DSC curve in the temperature range from 1388 K to 1503 K (Fig. 4). No titanium silicides were observed and no $CeSi_x$ remained. In addition, no silicon was detected in the reaction products of the CeO_2 and $CeCl_xO_y$ particles by EDS (see Fig. 5d and 5e). This suggests that the amount of Si introduced from $CeSi_2$ (0.14 wt% Si from an addition of 0.5 wt% $CeSi_2$) has all gone into solid solution. At the sintering temperature of 1623 K, the solubility of Si in β-Ti is ~3.6 wt%. After the β→α transformation during cooling, α-Ti can still contain ~0.45 wt% Si, which is greater than the Si content introduced. This explains why the Si introduced has all gone into solid solution. Although the exact details are unclear, the main reactions may be proposed as follows:

$$CeSi_2 \rightarrow CeSi_x + Si \quad (1)$$

$$Si \rightarrow [Si]_{Ti} \quad (2)$$

$$CeSi_x + [O]_{Ti} \rightarrow CeO_2 + [Si]_{Ti} \quad (3)$$

where $[O]_{Ti}$ and $[Si]_{Ti}$ represent the oxygen and silicon in solid solution in β-Ti during sintering, respectively. The formation of $CeCl_xO_y$ is limited because of the trace amount of Cl (≤500 ppm) in the Ti powder and is therefore not included.

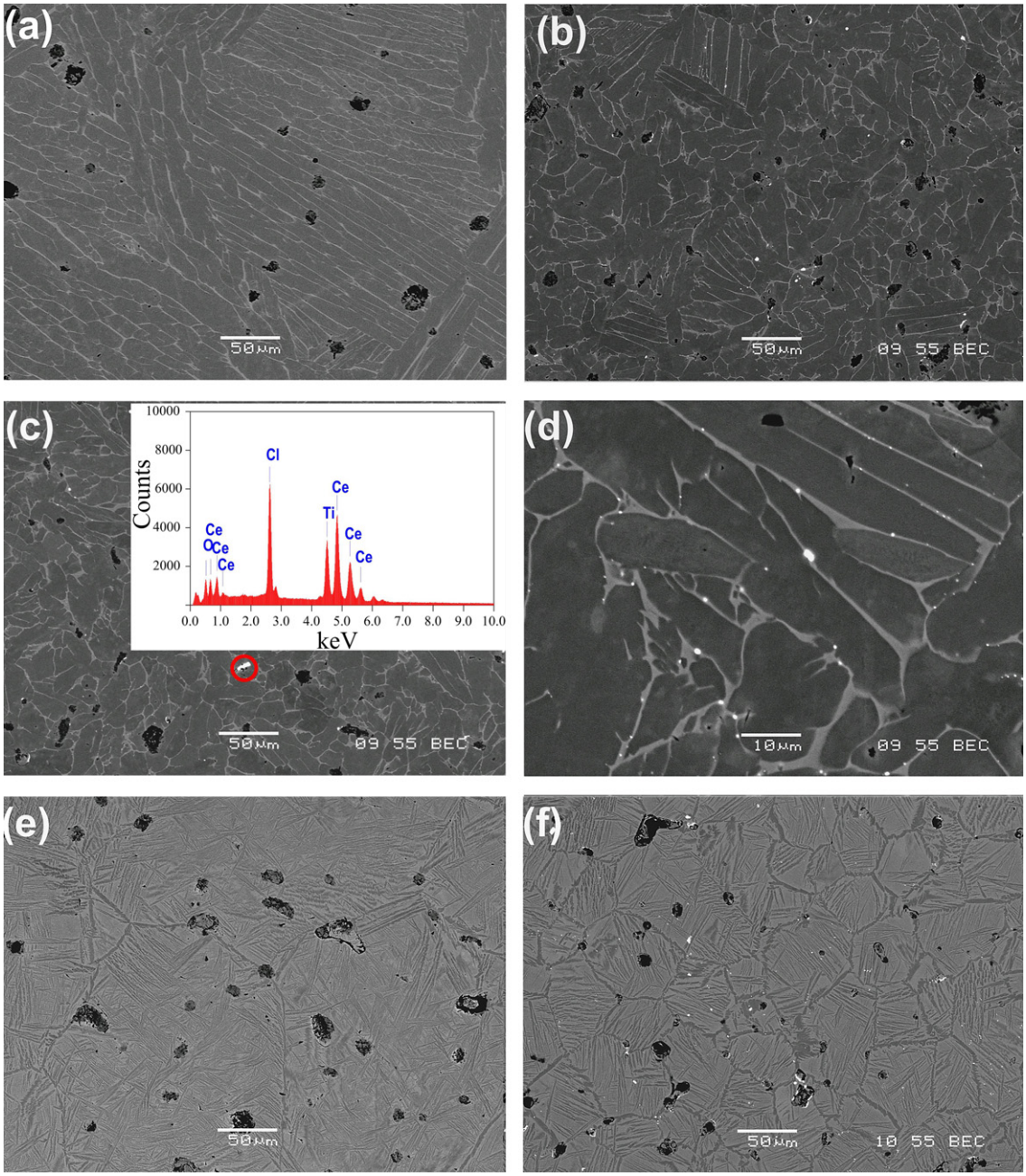

Fig. 6. Microstructural refinement of as-sintered Ti–6Al–4V and Ti–10V–2Fe–3Al by $CeSi_2$: (a) Ti–6Al–4V, (b) Ti–6Al–4V–0.5$CeSi_2$; (c) Ti–6Al–4V–0.7$CeSi_2$, (d) enlarged view of (c), (e) Ti–10V–2Fe–3Al and (f) Ti–10V–2Fe–3Al–0.5$CeSi_2$. Sintering was conducted at 1623 K for 120 min.

4.3. The microstructural refinement by Ce

An addition of Si can refine the microstructure of a PM alloy when stable titanium silicides form along the grain boundary [45,46]. As pointed out earlier, no silicides were found in the as-sintered Ti alloys because the Si content introduced is less than the solubility of Si in both β-Ti and α-Ti. The significant microstructural refinement observed is thus caused by Ce. This can be attributed to the formation of Ce-containing particles in the grain boundary area (see Fig. 5). They can effectively restrict the prior-β grain growth by pinning the grain boundaries. The use of a stable compound, particularly RE oxide particles such as Y_2O_3 and Dy_2O_3, as a β grain growth inhibitor in PM Ti alloys has long been recognized in order to avoid excessive prior-β grain growth [51]. The CeO_2 particles that form in situ in PM Ti materials during sintering are effective β grain growth inhibitors. Consequently, there was limited β grain growth due to the addition of $CeSi_2$. The refinement of the α-Ti laths stems from the refinement of the prior-β grains in which they nucleated and grew upon cooling.

4.4. The effect of $CeSi_2$ on tensile properties

The tensile strength of a titanium alloy is sensitive to its oxygen content in solid solution. Due to the formation of CeO_2 and $CeCl_xO_y$, the actual oxygen content in solid solution in the Ti matrix has decreased. This weakens the solid solution strengthening effect of oxygen and should have resulted in a decrease of the tensile strength. However, the dispersion strengthening from the

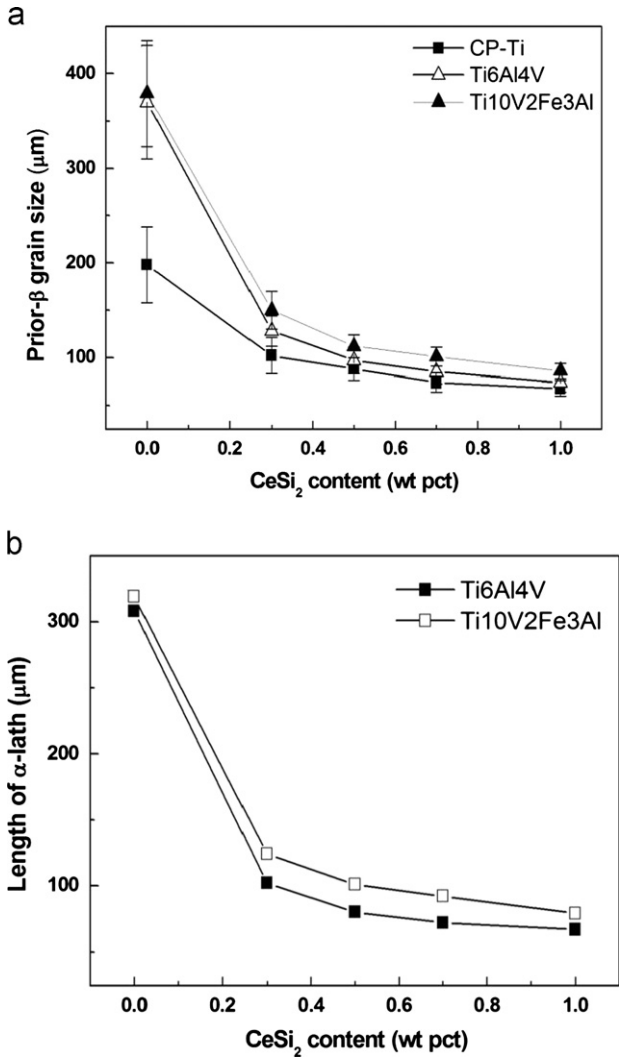

Fig. 7. (a) Prior-β grain size and (b) average length of the α-Ti laths of as-sintered CP-Ti, Ti–6Al–4V and Ti–10V–2Fe–3Al versus the addition of $CeSi_2$ (sintered at 1623 K for 120 min).

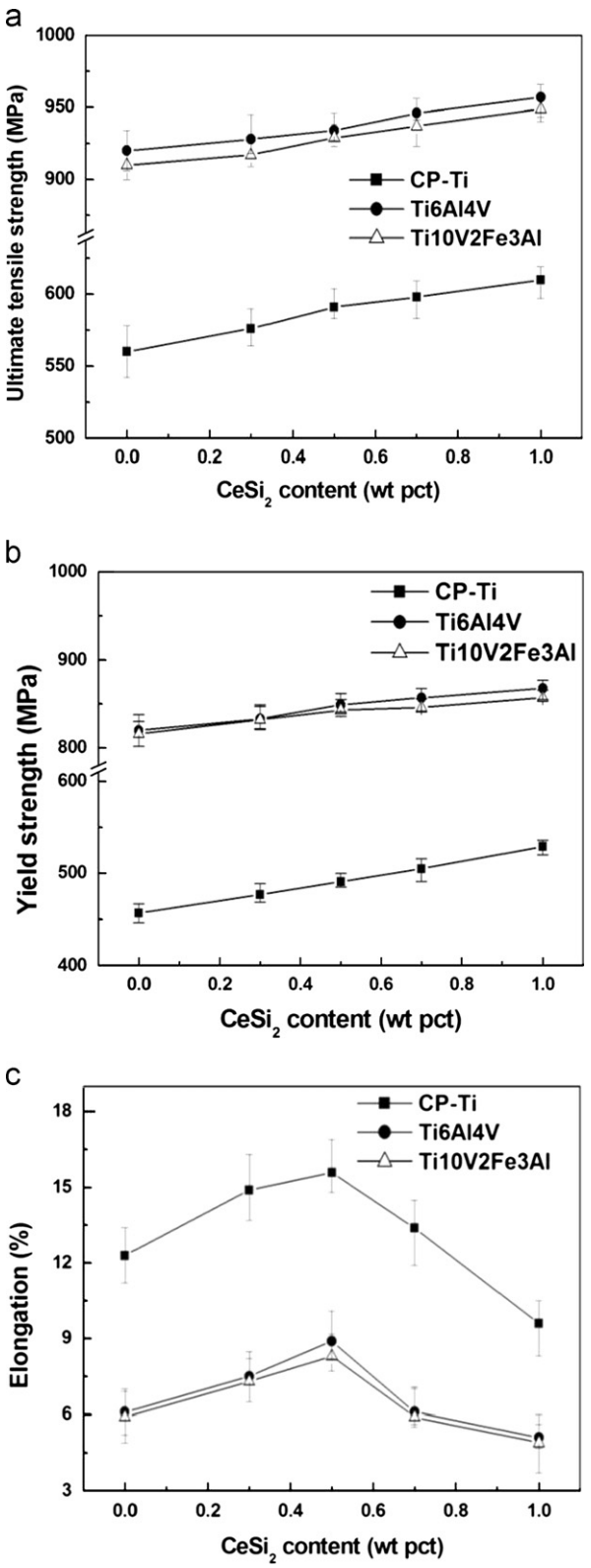

Fig. 8. (a) Ultimate tensile strength, (b) yield strength (0.2% offset) and (c) elongation of CP-Ti, Ti–6Al–4V and Ti–10V–2Fe–3Al versus the addition of $CeSi_2$, sintered at 1623 K for 120 min.

Ce-containing dispersoids and the solid solution strengthening of Si contributed to the strengthening. This, in conjunction with the microstructure refinement by Ce-containing particles and the improved density outweighed the loss of strength by the scavenging of oxygen leading to a marginal increase in the tensile strength (Fig. 8a and b). However, the scavenging of O should be the major reason for the enhanced ductility when the addition of $CeSi_2$ is ≤0.5 wt% (see Fig. 8c), together with the beneficial effect of the improved sintered. Increasing the addition of $CeSi_2$ beyond 0.5 wt% resulted in decreased sintered densities and the formation of coarse CeO_2 particles (see Fig. 6b and c). Their combined effects are responsible for the decreased ductility. In particular, the CeO_2 oxide particles are readily visible on the tensile fracture surfaces with many dimples containing coarse CeO_2 particles (see Fig. 9e). This directly links the drop in the tensile elongation to the addition of ≥0.5 wt% $CeSi_2$.

5. Summary

- $CeSi_2$ can be a practical form of Ce addition to PM Ti alloys for the scavenging of oxygen. An addition of ≤0.5 wt% $CeSi_2$ to CP-Ti, Ti–6Al–4V and Ti–10V–2Fe–3Al results in substantial microstructural refinement, improved tensile elongation and marginally increased sintered densities.

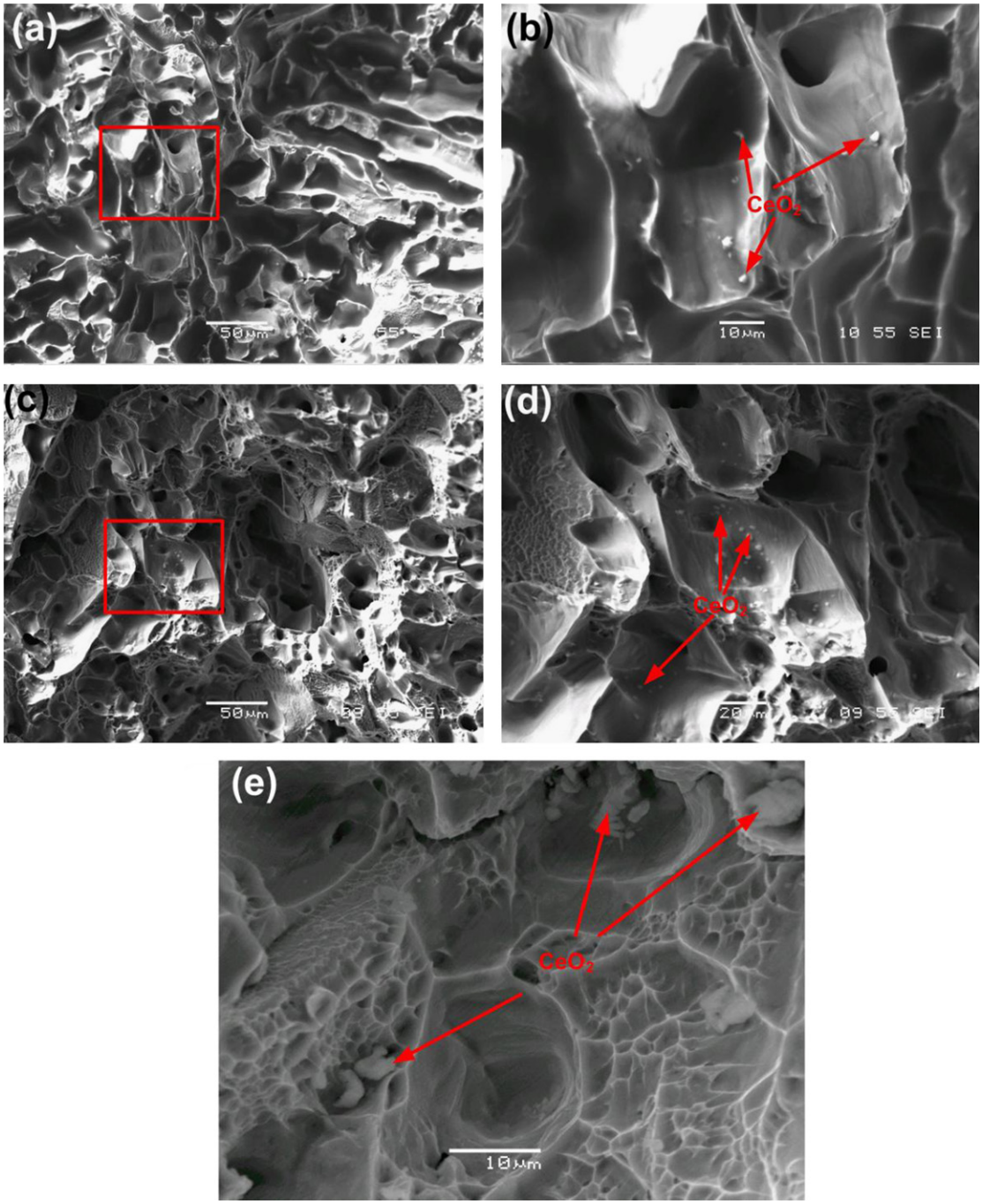

Fig. 9. (a) Fractograph of CP-Ti with an addition of 0.5 wt% $CeSi_2$ and (b) a magnified view of (a); (c) fractograph of Ti–6Al–4V with an addition of 0.5 wt% $CeSi_2$ and (d) a magnified view of (c); and (e) fractograph of Ti–6Al–4V with an addition of 0.7 wt% $CeSi_2$.

- The addition of $CeSi_2$ to CP-Ti, Ti–6Al–4V and Ti–10V–2Fe–3Al up to 1.0 wt% leads to the formation of both CeO_2 and $CeCl_xO_y$ compounds. The Si passes completely into solid solution in the titanium matrix. Ce can simultaneously scavenge O and Cl from the titanium matrix during sintering.
- The stable CeO_2 and $CeCl_xO_y$ particles are effective β-Ti grain growth inhibitors. They form along or close to the grain boundary and are responsible for the substantial microstructural refinement of the prior-β grains and the subsequent α-laths.
- The small improvement in the sintered density by an addition of ≤0.5 wt% $CeSi_2$ is caused by the Si rather than the Ce. An addition of >0.5 wt% $CeSi_2$ leads to a significant drop in the sintered density, despite the favorable effect of the increased Si content on the sintering densification.
- The optimum addition level of $CeSi_2$ is about 0.5 wt%, beyond which the tensile elongation drops due to a decrease in sintered density and the formation of coarse CeO_2 particles.

Acknowledgments

This work was funded by the Australian Research Council (ARC) through an Australian Postdoctoral Fellowship for Y.F. Yang and by The University of Queensland through an Early Career Researcher

Grant for Y.F. Yang. Support from the ARC Centre of Excellence for Design in Light Metals is also acknowledged. The authors also wish to acknowledge the constructive comments received from the reviewer.

References

[1] M. Qian, Int. J. Powder Metall. 46 (2010) 29–44.
[2] H. Nakajima, K. Yusa, Y. Kondo, Scr. Mater. 34 (1996) 249–253.
[3] Z.Z. Fang, Int. J. Powder Metall. 46 (2010) 9–17.
[4] H. Miura, Key Eng. Mater. 520 (2012) 30–40.
[5] O.M. Ferri, T. Ebel, R. Bormann, Adv. Eng. Mater. 13 (2011) 436–447.
[6] H.J.T. Ellingham, J. Soc. Chem. Ind. 63 (1994) 125–133.
[7] M. Hansen, Constitution of Binary Alloys, McGraw-Hill, New York, 1958.
[8] R.P. Ellion, Constitution of Binary Alloys, 1st Supplement, McGraw-Hill, New York, 1965.
[9] B.B. Rath, R.J. Lederich, J.E. O'Neal, Grain Boundaries in Engineering Materials, in: J.L. Walter, J.H. Westbrook, D.A. Woodford (Eds.), Claitor's Publishing Division, Baton Rouge, LA, 1975, p. 39.
[10] J.E. O'Neal, S.M.L. Sastry, R.J. Lederich, Microstructural Science, in: P.A. Fallon, J. L. McCall (Eds.), Elsevier, New York, NY, 1979, p. 159.
[11] K.K. Sankaran, S.M.L. Sastry, J.E. O'Neal, Metall. Trans. A 11A (1980) 196–198.
[12] B.B. Rath, J.E. O'Neal, R.J. Lederich, Proceedings of the Electron Microscopy Society of America, Claitors Publishing Division, Baton Rouge, LA, 1974.
[13] J.E. O'Neal, S.M.L. Sastry, R.J. Lederich, Proceedings of the 11th International Metallographic Convention, Elsevier, New York, NY, 1979.
[14] D.G. Konitzer, B.C. Muddle, H.L. Fraser, Scr. Metall. 17 (1983) 963–966.
[15] S.M.L. Sastry, P.J. Meschter, J.E. O'Neal, Metall. Trans. A 15 (1984) 1451–1463.
[16] S.M.L. Sastry, P.J. Meschter, J.E. O'Neal, R.J. Lederich, B.B. Rath, J. Mater. Sci. 14 (1979) 179–183.
[17] S.M.L. Sastry, T.C. Peng, L.P. Beckerman, Metall. Trans. A 15A (1984) 1465–1474.
[18] S. Naka, M. Marty, H. Octor, J. Mater. Sci. 22 (1987) 887–895.
[19] F.H. Froes, R.G. Rowe, Proceedings of the Symposium held at the 1986 TMS-AIME Annual Meeting, New Orleans, LA, USA, 1986.
[20] D.B. Snow, A.F. Anthony, Proceedings of the Symposium held at the 1986 TMS-AIME Annual Meeting, New Orleans, LA, USA, 1986.
[21] J.P.A. Lofvander, S.A. Court, R. Wheeler, J.W. Sears, D.A. Watson, H.L. Fraser, Proceedings of the Symposium held at the 1986 TMS-AIME Annual Meeting, New Orleans, LA, USA, 1986.
[22] R.E. Anderson, J.L. Larson, Proceedings of the Symposium held at the 1986 TMS-AIME Annual Meeting, New Orleans, LA, USA, 1986.
[23] D.B. Snow, Proceedings of the Symposium held at the 1986 TMS-AIME Annual Meeting, New Orleans, LA, USA, 1986.
[24] D.B. Snow, A.F. Giamei, Proceedings of the Symposium held at the 1986 TMS-AIME Annual Meeting, New Orleans, LA, USA, 1986.
[25] Y.D. Hahn, D. Vujic, S.H. Whang, Proceedings of the Symposium held at the 1986 TMS-AIME Annual Meeting, New Orleans, LA, USA, 1986.
[26] C. Suryanarayana, F.H. Froes, JOM 42 (1990) 22–25.
[27] D.G. Konitzer, J.P.A. Lofvander, S.A. Court, R. Kirchheim, H.L. Fraser, Acta Metall. 36 (1988) 1595–1606.
[28] D.G. Konitzer, J.T. Stanley, M.H. Loretto, H.L. Fraser, Acta Metall. 34 (1986) 1269–1277.
[29] F.H. Froes, D. Eylon (Eds.), The Metallurgical Society, Warrendale, PA, 1986.
[30] S.A. Court, J.T. Stanley, D.G. Konitzer, M.H. Loretto, H.L. Fraser, Acta Metall. 36 (1988) 1585–1594.
[31] J.P.A. Lofvander, S.A. Court, R. Kirchheim, H.L. Fraser, Scr. Metall. 21 (1987) 859–861.
[32] M.F.X. Gigliotti, A.P. Woodfield, Metall. Trans. A 30 (1992) 1761–1771.
[33] K. Xia, W. Li, C. Liu, Scr. Mater. 41 (1999) 67–71.
[34] E. Bouchaud, J.P. Bouchaud, S. Naka, G. Lapasset, H. Octor, Acta Metall. Mater. 40 (1992) 3451–3458.
[35] H.P. Tang, B.Y. Huang, H.Y. Liu, Z.Y. Huang, Y. Liu, H.W. Ouyang, Rare Met. Mater. Eng. 33 (2004) 43–46.
[36] Y. Liu, L.F. Chen, W. Wei, H.P. Tang, C.T. Liu, B. Liu, B.Y. Huang, J. Mater. Sci. Technol. 22 (2006) 465–469.
[37] F.Y. Zhang, J. Chen, H. Tan, X. Lin, W.D. Huang, Rare Met. Mater. Eng. 36 (2007) 1420–1424.
[38] Y. Liu, B. Wang, J. Qiu, H. Tang, Mater. Manuf. Processes 25 (2010) 735–739.
[39] B. Wang, Y. Liu, Y.B. Liu, H.P. Tang, J.W. Jing, Y.L. Wang, Mater. Sci. Eng. Powder Metall. 16 (2011) 136–142, in Chinese.
[40] Y. Liu, Y.B. Liu, B. Wang, H.P. Tang, Key Eng. Mater. 520 (2012) 41–48.
[41] B. Liu, Y.P. Li, H. Matsumoto, Y.B. Liu, Y. Liu, A. Chiba, Mater. Sci. Eng. A 528 (2011) 2345–2352.
[42] M. Yan, Y. Liu, Y.B. Liu, C. Kong, G.B. Schaffer, M. Qian, Scr. Mater. 67 (2012) 491–494.
[43] M. Yan, Y. Liu, G.B. Schaffer, M. Qian, Scr. Mater. 68 (2013) 63–66.
[44] Alfa Aesar, ⟨www.alfa.com⟩ [Accessed 30 October 2012].
[45] Y.F. Yang, S.D. Luo, G.B. Schaffer, M. Qian, Mater. Sci. Eng. A 528 (2011) 7381–7387.
[46] Y.F. Yang, S.D. Luo, G.B. Schaffer, M. Qian, Metall. Mater. Trans. A 43 (2012) 4896–4906.
[47] Y.F. Yang, S.D. Luo, G.B. Schaffer, M. Qian, Mater. Sci. Eng. A 528 (2011) 6719–6726.
[48] F. Benesovsky, H. Nowotny, W. Rieger, H. Rassaert, Monatsh. Chem. 97 (1966) 221–229 (in German).
[49] A. Munitz, A.B. Gokhale, G.J. Abbaschian, Bull. Alloy Phase Diagrams 10 (1989) 73–78.
[50] R. Vogel, Z. Anorg. Chem. 84 (1913) 323–339 (in German).
[51] M. Marty, H. Octor, A. Walder, US Patent, 4, 601, 874 (filed 8 July 1985, granted 22 July 1986).